EARTHQUAKE ENGINEERING AND STRUCTURAL DYNAMICS
Earthquake Engng Struct. Dyn. 2009; **38**:1381–1399
Published online 23 February 2009 in Wiley InterScience (www.interscience.wiley.com). DOI: 10.1002/eqe.907

A substructure shaking table test for reproduction of earthquake responses of high-rise buildings

Xiaodong Ji[1,*,†], Kouichi Kajiwara[2], Takuya Nagae[2], Ryuta Enokida[1] and Masayoshi Nakashima[1]

[1]*Disaster Prevention Research Institute, Kyoto University, Gokasho, Uji, Kyoto 611-0011, Japan*
[2]*E-Defense, National Research Institute for Earth Science and Disaster Prevention, Shinjimicho, Miki, Hyogo 673-0515, Japan*

SUMMARY

When subjected to long-period ground motions, high-rise buildings' upper floors undergo large responses. Furniture and nonstructural components are susceptible to significant damage in such events. This paper proposes a full-scale substructure shaking table test to reproduce large floor responses of high-rise buildings. The response at the top floor of a virtual 30-story building model subjected to a synthesized long-period ground motion is taken as a target wave for reproduction. Since a shaking table has difficulties in directly reproducing such large responses due to various capacity limitations, a rubber-and-mass system is proposed to amplify the table motion. To achieve an accurate reproduction of the floor responses, a control algorithm called the open-loop inverse dynamics compensation via simulation (IDCS) algorithm is used to generate a special input wave for the shaking table. To implement the IDCS algorithm, the model matching method and the H_∞ method are adopted to construct the controller. A numerical example is presented to illustrate the open-loop IDCS algorithm and compare the performance of different methods of controller design. A series of full-scale substructure shaking table tests are conducted in E-Defense to verify the effectiveness of the proposed method and examine the seismic behavior of furniture. The test results demonstrate that the rubber-and-mass system is capable of amplifying the table motion by a factor of about 3.5 for the maximum velocity and displacement, and the substructure shaking table test can reproduce the large floor responses for a few minutes.

Received 18 August 2008; Revised 17 January 2009; Accepted 20 January 2009

KEY WORDS: shaking table test; substructure; IDCS algorithm; model matching method; H_∞ method; high-rise building

*Correspondence to: Xiaodong Ji, Disaster Prevention Research Institute, Kyoto University, Gokasho, Uji, Kyoto 611-0011, Japan.
†E-mail: xiaodong.ji@ks5.ecs.kyoto-u.ac.jp

1. INTRODUCTION

A long-period, long-duration ground motion induced by a subduction earthquake in the Pacific ocean-ridge zone is expected to attack Japan in the next few decades with a very high probability [1]. High-rise buildings are prone to sustain significant responses characterized by many cycles of vibrations with large velocities and displacements. Two types of damages are likely to occur in such events. Beam-to-column connections are susceptible to serious low-cycle fatigue failures resulting from many cycles of plastic deformations [2]. Furniture and nonstructural components in top stories are likely to be shaken significantly, resulting in sliding, falling, overturning, and collisions of these elements [3].

To examine the seismic behavior of furniture under large floor responses, large-scale tests are a must, because it is very difficult to make reduced-size furniture without the loss of similitude. Apparently, a full-scale test of a high-rise building as a whole is impracticable. One alternative is the application of the online hybrid test, which is capable of handling a large-scale structure by the introduction of substructuring techniques [4–8]. The test, however, adopts quasi-static loading, which is not feasible in the simulation of sliding and overturning behavior of furniture. Recently, the real-time hybrid test has been explored extensively [9–13], but the development is yet in its infancy, and the application is limited to simple structures loaded by smaller actuator devices.

Another alternative is a substructure shaking table test using large-scale shaking table facilities. The simple way is to extract the top portion of a high-rise building as a test specimen and use the floor response of that portion as the table input motion. Unfortunately, this is also unfeasible in most cases due to the limitations of various capacities associated with the shaking table, e.g. the capacities of the maximum displacement and velocity, and the amount of oil supply.

To overcome these difficulties, this paper proposes a new full-scale substructure shaking table test. Three inventions are included in this effort. One is the substructuring, and only a portion of the structure instead of the entire structure is physically tested on the table. Another is the introduction of a rubber-and-mass system to amplify the motion of the shaking table, and the last is the development of a control algorithm to generate a special input wave that can reproduce the floor response on the test specimen. A schematic view of the substructure shaking test is shown in Figure 1, in which the top floor is physically tested, while the lower portions are replaced by two layers of rubber-and-mass structures. With substructuring, the tested structure can maintain a

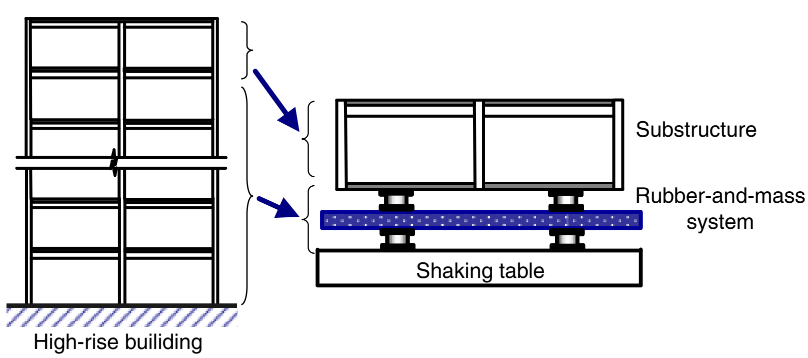

Figure 1. Rubber-and-mass system and substructure.

DOI: 10.1002/eqe

reasonable scale, and the rubber-and-mass system serves as an amplifier. Because of the nonlinear nature of the prototype high-rise building, the input wave of the shaking table has to be chosen carefully even if the rubber layers are linearly elastic.

The paper consists of four parts. First, a virtual 30-story steel building is introduced, and the response of the top floor of this building when subjected to a long-period, long-duration ground motion is presented. This response becomes a target response to be reproduced on the test specimen. Second, a control algorithm, i.e. the open-loop inverse dynamics compensation via simulation (IDCS) algorithm, is presented for the identification of the table motion that can reproduce the target response. For design of the controller, two methods, the model matching method and the H_∞ method, are adopted. Third, the effectiveness of the control algorithm is calibrated against a numerical example for a two Degrees of freedom (DOFs) system. Fourth, physical shaking table tests are implemented for the validation of the proposed full-scale substructure shaking table test, and behavior of and damage to furniture are discussed.

2. NONLINEAR TIME HISTORY ANALYSIS OF A HIGH-RISE BUILDING MODEL

2.1. Numerical model of a high-rise building and ground motion

A virtual 30-story building was considered in this study. The heights of the first story and the other stories were 4.2 and 3.4 m, respectively, and the total height of the building was 102.8 m. A lumped mass and shear spring model was adopted to simulate earthquake responses of the building, in which the lumped mass represented the story mass, and the shear spring represented the story stiffness. The parameters of the model were determined according to standard practices of seismic design in Japan. All story masses were assigned with an identical weight of 1000 tons, and the distribution of the initial story stiffness along the height was taken to follow the design story shear distribution. Nonlinearity of the story stiffness was described by a tri-linear kinematic hardening model with a skeleton curve as shown in Figure 2, in which F, Δ, and k_1 denoted the story shear force, story drift, and initial stiffness, respectively. The shear forces at the first and second yielding points were assumed as 1.2 and 2.0 times the designed yield strength (Q_d), and the second and third stiffness after yielding was assumed to be 0.7 and 0.1 times the initial stiffness, respectively. The fundamental natural period of the building was estimated as 2.8 s and the damping ratio was assigned to be 2% for the first mode. The building was subjected to ground motions in two horizontal directions, and the same numerical model was adopted for both the directions.

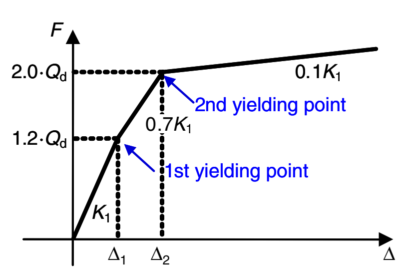

Figure 2. Skeleton curve of story restoring force behavior.

Earthquake Engng Struct. Dyn. 2009; **38**:1381–1399
DOI: 10.1002/eqe

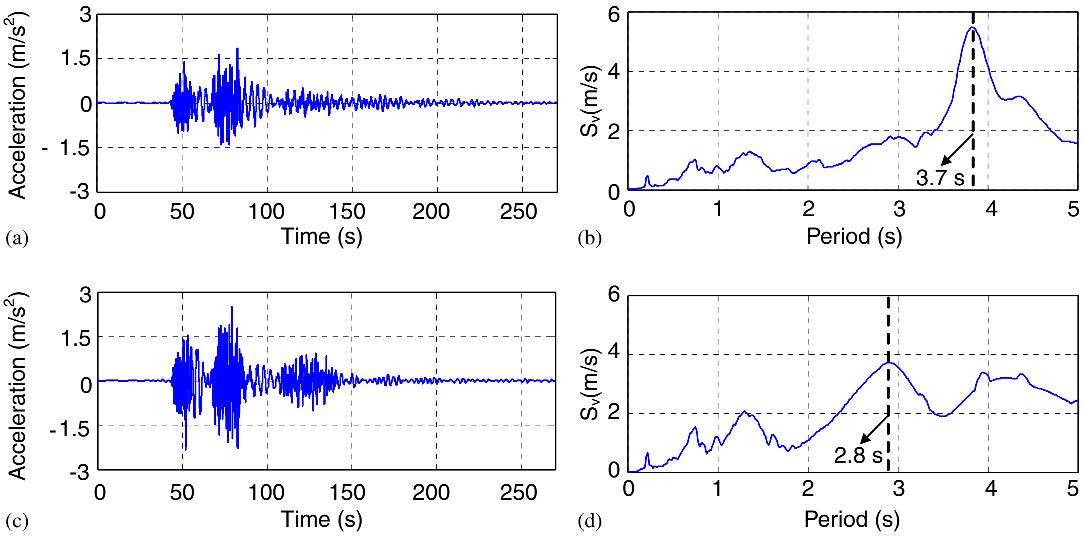

Figure 3. HigashiYuuenchi ground motion: (a) time history in EW direction; (b) velocity response spectrum in EW direction; (c) time history in NS direction; and (d) velocity response spectrum in NS direction.

A synthesized long-period, long-duration ground motion named HigashiYuuenchi ground motion was adopted as the input excitation, as shown in Figure 3 [14]. The ground motion was estimated based on a hypothetical Nankai earthquake (M8.4), with a rupture length of 180 km and a focus depth of 10 km. The ground motion has a duration of 270 s, and predominant periods of 3.7 and 2.8 s in the EW and NS direction, respectively. The peak ground acceleration (PGA) values are 184 and 249 m/s^2, and the peak ground velocity (PGV) values are 0.42 and 0.73 m/s in the two horizontal directions.

2.2. Earthquake response of the high-rise building

The Newmark-β method ($\beta = 0.25$ and $\gamma = 0.5$) was used for the time integration to achieve the necessary responses. In the HigashiYuuenchi ground motion, the maximum story drift angles occur in the third story, reaching 0.83 and 1.68% in the EW and NS direction, with the associated story ductility of 2.0 and 4.1. The peak values of the acceleration, velocity, and displacement of the top floor are 3.82 m/s^2, 1.54 m/s and 0.93 m in the EW direction, and 4.20 m/s^2, 2.15 m/s and 1.24 m in the NS direction. The time histories of the acceleration responses at the top floor and the corresponding Fourier amplitude spectra are shown in Figure 4. The predominant frequencies of the floor responses are 0.35 and 0.34 Hz in the EW and NS direction, respectively, exhibiting a notable long-period motion. Owing to the long-period, long-duration vibration, the cumulative displacement at the top floor reaches about 180 m.

To investigate the furniture behavior, a simple way is to extract the top story as a test substructure and directly use the top floor's response as the table input. The associated test demands for such direct reproduction are shown in Table I. Table I also shows the capacities of the Hyogo Earthquake Engineering Research Center (E-Defense) facility, featuring a table of 20 m by 15 m in the plan [15, 16]. The table is actuated in 3D and can accommodate a specimen up to a weight of 12 MN.

DOI: 10.1002/eqe

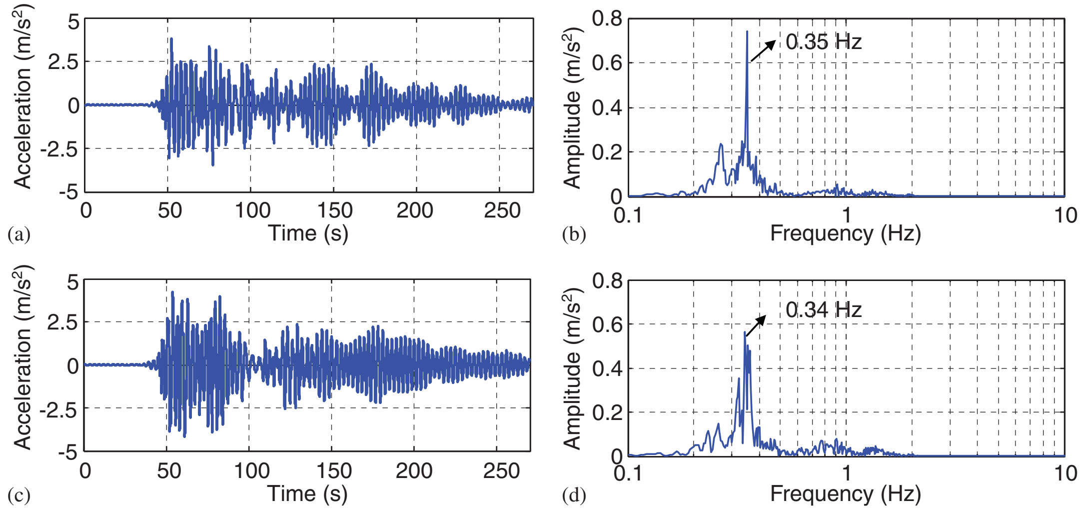

Figure 4. Acceleration responses of top floor: (a) time history in EW direction; (b) Fourier amplitude spectrum in EW direction; (c) time history in NS direction; and (d) Fourier amplitude spectrum in NS direction.

Table I. Demands for direct reproduction and capacities of E-Defense's shaking table.

	Demand	Capacity
Acceleration (m/s^2)	4.20	9.0
Velocity (m/s)	2.15	2.0
Displacement (m)	±1.24	±1.0
Oil amount (kl)	306	20.0

The specification limits of the maximum acceleration, velocity, and displacement of the table are $9.0\,m/s^2$, 2.0 m/s, and ±1.0 m. The amount of oil required is related to the cumulative displacement of the shaking table. The oil supply is normally capped because of the accumulator used for the table facility.

As evidenced in Table I, the expected floor response cannot be used as the direct input, because its maximum velocity and displacement exceed the capacity limits of the E-Defense table by 7.5 and 24.0%, and the amount of oil required is about 15 times the oil supply limit.

To overcome these limitations, a rubber-and-mass system is proposed, which is set beneath the test substructure model to amplify the motion of the shaking table. The rubber-and-mass system consists of multiple rubber layers and lumped masses. Rubber bearings are adopted because of their stable elastic behavior. The number of rubber layers is determined according to the displacement demand and the deformation capacity of each rubber layer. By a suitable design of the stiffness of rubber layers and the weight of masses, the entire test specimen that comprises the substructure model and rubber-and-mass system is able to achieve linear dynamic properties similar to those of the prototype building. However, nonlinearity of the prototype cannot be reflected by the test specimen, because the rubber-and-mass system works nearly elastically. To achieve an accurate

DOI: 10.1002/eqe

reproduction of the top floor's response, it becomes imperative to generate a special input wave for the shaking table, rather than to directly use the original ground motion itself.

3. CONTROL ALGORITHMS

3.1. IDCS algorithm

Identification of an input wave from a target response belongs to an inverse dynamics problem. Real-time adaptive control approaches, for example, the minimal control synthesis (MCS) method [17], have a strong potential of solving the inverse problem and allowing for the specimen's nonlinearity. To date, however, real-time adaptive control is still in the stage of development, and applications have been limited to relatively simple structures shaken by rather small shaking tables. On reflecting in the lack of maturity of the concerned technologies, the writers felt that the risk would be too high yet for the large and complex shaking table used in this study (weighing close to 20 MN (2000 ton) and controlled in 6DOFs) to adopt a real-time adaptive control strategy. For this reason, a more robust, stable, and safer offline control approach, named the IDCS algorithm, is adopted to generate the input wave of the shaking table. The basic idea of the open-loop IDCS algorithm is to generate a special wave from a numerical feedback loop and to control the behavior of a physical specimen by this wave [18, 19].

A block diagram description of the open-loop IDCS algorithm is given in Figure 5, in which B_e represents the test specimen; B represents the numerical model of B_e; W denotes the controller; r represents the target wave, i.e. the response of the top floor; u represents the input wave of the shake table; y_e denotes the specimen's response; and y denotes the calculated response by the numerical model. The wave u can be obtained from the numerical loop. It is expected that if the numerical model B accurately represents the test specimen B_e, the real response y_e of the test specimen under the excitation of the generated input wave u should be sufficiently close to the response y of the numerical model. That is, a good controller W, designed to ensure that y tracks r well, promises a reproduction. To implement the IDCS algorithm, the model matching method and the H_∞ method are adopted, since they show good performance in controller design for linear time-invariant systems [20, 21].

3.2. Model matching method

The model matching method is a classical method of the controller design for linear systems. The so-called model matching means to determine a controller so that the transfer function of the feedback system coincides exactly with the expected function. The frequency domain model matching method is used in this paper, because it is simpler and more convenient in the computational work than the time domain model matching method [20].

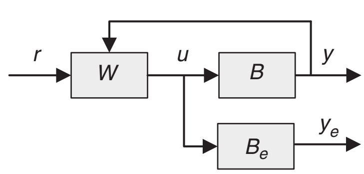

Figure 5. Principle of open-loop IDCS algorithm.

DOI: 10.1002/eqe

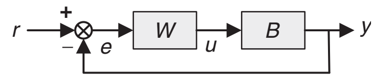

Figure 6. Feedback control system.

Consider a general block diagram for the feedback control system given in Figure 6, in which the model B is also called the plant, and e represents the error between the system input r and the system output y. Let the transfer functions of the plant B and controller W, $T_B(s)$ and $T_W(s)$, be expressed by

$$T_B(s) = \frac{N_B(s)}{M_B(s)} \tag{1}$$

$$T_W(s) = \frac{N_W(s)}{M_W(s)} \tag{2}$$

in which $N_B(s)$ and $N_W(s)$ denote the numerator polynomials of the plant B and controller W, and $M_B(s)$ and $M_W(s)$ denote their corresponding denominator polynomials. The transfer function of the feedback system, i.e. the transfer function from r to y can be obtained as follows:

$$T_{ry}(s) = \frac{T_W(s)T_B(s)}{1+T_W(s)T_B(s)} = \frac{N_W(s)N_B(s)}{M_W(s)M_B(s)+N_W(s)N_B(s)} \tag{3}$$

To ensure that y accurately tracks r, the transfer function $T_{ry}(s)$ should equal unity in the concerned frequency range. The polynomials $N_B(s)$ and $M_B(s)$ can be calculated from state-space matrices of the plant systematically. Herein the degrees of $N_B(s)$ and $M_B(s)$ are denoted as n_B and m_B, respectively. The polynomials of the controller, $N_W(s)$ and $M_W(s)$, are designated to be of degrees of n_W and m_W. n_W and m_W should be larger than n_B and m_B, respectively, and the difference between n_W and m_W should be equal to the difference between n_B and m_B. By reasonably assigning poles of the denominator polynomial of the transfer function $T_{ry}(s)$, the magnitude of transfer function $T_{ry}(s)$ approaches unity. Then, the coefficients of polynomials, $N_W(s)$ and $M_W(s)$, can be determined by the Bott–Duffin inverse operation [22].

Although the model matching method is comprehensive in theory and simple in computation, some drawbacks exist in application, e.g. the assignment of suitable poles has to rely on the experience of the controller designer, and trials and errors are required to obtain a good solution.

3.3. H_∞ method

The H_∞ method receives much attention due to its distinguished capability of designing an optimal robust controller [21, 23]. In this paper, the H_∞ mixed sensitivity method is used to construct a controller. To represent the sensitivity of a feedback control system with respect to the external disturbance and the plant's uncertainty, the sensitivity function and the compensation sensitivity function are defined, respectively, as follows:

$$S(s) = T_{re}(s) = \frac{1}{1+T_W(s)T_B(s)} \tag{4}$$

$$T(s) = T_{ry}(s) = \frac{T_W(s)T_B(s)}{1+T_W(s)T_B(s)} \tag{5}$$

DOI: 10.1002/eqe

in which $S(s)$ is the sensitivity function, i.e. the transfer function from r to e, and $T(s)$ is the compensation sensitivity function, i.e. the transfer function from r to y. To attenuate the adverse influence of external disturbance and plant's uncertainty, functions $S(s)$ and $T(s)$ should be minimized. However, minimization of $S(s)$ and $T(s)$ cannot be achieved simultaneously for the same frequency, since the sum of them is unity at any frequency value. Two weighting functions $W_S(s)$ and $W_T(s)$ are thus introduced to construct a mixed-sensitivity optimization problem. A mixed-sensitivity cost function that penalizes both $S(s)$ and $T(s)$ is minimized as follows [24]:

$$\left\| \begin{matrix} W_s(s)\cdot S(s) \\ W_T(s)\cdot T(s) \end{matrix} \right\|_\infty \leqslant \gamma \tag{6}$$

in which, γ is a small positive value and $\| \|_\infty$ denotes the infinity norm of matrix [25]. Solving Equation (6) by using the improved loop-shifting two-Riccati formulas [26], the transfer function of the controller W can be obtained.

Although the theory and computation appear rather complicated, the H_∞ method is convenient for application, because the mixed-sensitivity problem can be solved systematically by the robust control toolbox of the software Matlab [27]. Since the performance of the constructed controller is related to weighting functions, it is noted that care must be taken to select these weighting functions. Selection of weighting functions depends on the experience of the controller designer, and the design involves trials and errors until the feedback system meets its design specifications [24].

4. NUMERICAL ILLUSTRATION

4.1. Numerical model

A numerical example is presented to illustrate the feasibility of the open-loop IDCS algorithm and compare the performance of the model matching method with the H_∞ method. Since the test specimen described in the following section is simplified into a two DOFs model, the numerical example also chooses a model with two DOFs as shown in Figure 7. Consistent with the test specimen, the masses of m_1 and m_2 were assigned as 3.60×10^5 and 3.95×10^5 kg, and the stiffnesses of k_1 and k_2 were assigned as 5.548 and 3.511 MN/m, respectively. The damping matrix was assumed to be proportional to the stiffness matrix, and the first modal damping ratio was designated as 3%.

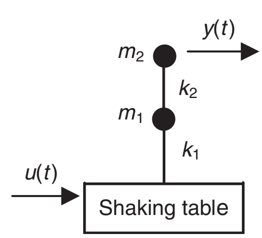

Figure 7. Numerical simulation model.

DOI: 10.1002/eqe

If the excitation acceleration of the shaking table and response accelerations of the model are taken as the input and output, the associated state-space equation can be written as

$$\begin{aligned}\dot{\boldsymbol{x}}(t) &= \boldsymbol{A}\boldsymbol{x}(t)+\boldsymbol{B}u(t)\\ \boldsymbol{y}(t) &= \boldsymbol{C}\boldsymbol{x}(t)\end{aligned} \tag{7}$$

in which the state vector $\boldsymbol{x}(t)=[\boldsymbol{d}(t)\ \ \dot{\boldsymbol{d}}(t)]^{\mathrm{T}}$ consists of the relative displacement vector $\boldsymbol{d}(t)$ and the relative velocity vector $\dot{\boldsymbol{d}}(t)$; $\boldsymbol{y}(t)$ denotes the output, i.e. the acceleration vector of the model; $u(t)$ denotes the input, i.e. the excitation acceleration of the shaking table; and the matrices $\boldsymbol{A}$, $\boldsymbol{B}$, and $\boldsymbol{C}$ represent the system matrix, control matrix and observation matrix, which can be constructed from the mass, damping, and stiffness matrices [28].

Transforming Equation (7) by the Laplace transform and then rearranging, the transfer function matrix of the numerical model can be obtained as

$$\boldsymbol{T}_B(s)=\boldsymbol{C}(s\boldsymbol{I}-\boldsymbol{A})^{-1}\boldsymbol{B} \tag{8}$$

where s denotes the Laplace variable. Substituting the parameters associated with the numerical model, the transfer function from the acceleration of the table to the acceleration response at the top floor is expressed as:

$$T_B(s)=\frac{0.106s^2+7.614s+136.983}{s^4+0.946s^3+34.158s^2+7.614s+136.983} \tag{9}$$

The Bode diagram of the transfer function is shown in Figure 8. The first two modal frequencies of the numerical model, f_1 and f_2, were 0.34 and 0.86 Hz.

4.2. Controller design

First, the model matching method was used to construct the controller. The denominator and numerator of the controller's transfer function $T_W(s)$ were assumed to be the polynomials of 6 and 4 degrees, respectively. Equation (3) indicates that the denominator of the transfer function of the feedback system was a polynomial of 10 degrees. Through trial and error, the poles of the denominator polynomial were assigned as $[0.5, 0.5, 0.7, 0.7, 5, 8, 30, 30, 40, 40]^{\mathrm{T}}$. Then coefficients

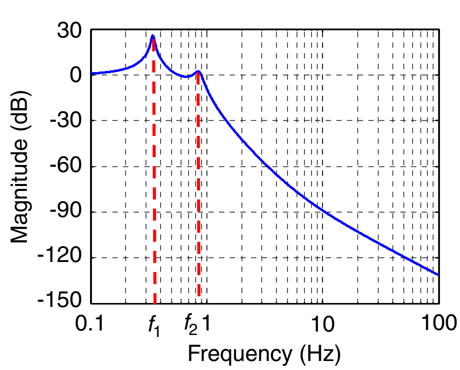

Figure 8. Transfer function of numerical model.

DOI: 10.1002/eqe

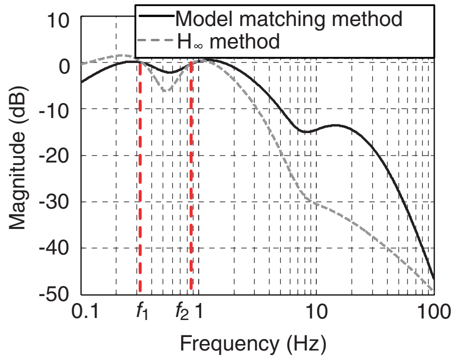

Figure 9. Transfer function of feedback system.

of the numerator and dominator polynomials of the controller's transfer function were calculated from the Bott–Duffin inverse operation. The Bode diagram of the transfer function of the feedback system is shown in Figure 9. It is notable that the magnitude of the transfer function is very close to unity at the natural frequencies of the plant.

To compare with the model matching method, the H_∞ method was also employed. To make the feedback system insensitive at the resonant frequencies of the plant, a notch function [28] was constructed as shown in Equation (10) to serve as the weighting function $W_s(s)$. On the other hand, to roll-off the control action at high frequencies where model uncertainties cannot be ignored, the weighting function $W_T(s)$ should be chosen to have a high-pass filter's property. Herein, the weighting functions are given by

$$W_s(s) = \frac{\alpha_1(s^2+2\widehat{h_1}\,\omega_1 s+\omega_1^2)}{s^2+2h_1\omega_1 s+\omega_1^2}\cdot\frac{\alpha_2(s^2+2\widehat{h_2}\,\omega_2 s+\omega_2^2)}{s^2+2h_2\omega_2 s+\omega_2^2} \tag{10}$$

$$W_T(s) = \beta s^2 \tag{11}$$

in which ω_1 and ω_2 are the first two circular frequencies of the plant; h_1 and h_2 are the first two modal damping ratios of the plant; and the other parameters are determined by trial and error as follows: $\alpha_1=\alpha_2=1.25$, $\widehat{h_1}=\widehat{h_2}=0.5$, $\beta=0.005$. Then the transfer function of the controller was obtained by solving Equation (6) using the improved loop-shifting two-Riccati formulas [26]. Figure 9 shows the Bode diagram of the transfer function of the feedback system, indicating that the magnitude of the transfer function at natural frequencies of the plant is close to unity.

4.3. Numerical simulation results

The top floor's response of the 30-story building is considered as the target wave r. The transfer function from the target wave r to the shaking table's input wave u is given by:

$$T_{ru}(s) = \frac{T_W(s)}{1+T_W(s)T_B(s)} = \frac{N_W(s)M_B(s)}{M_W(s)M_B(s)+N_W(s)N_B(s)} \tag{12}$$

DOI: 10.1002/eqe

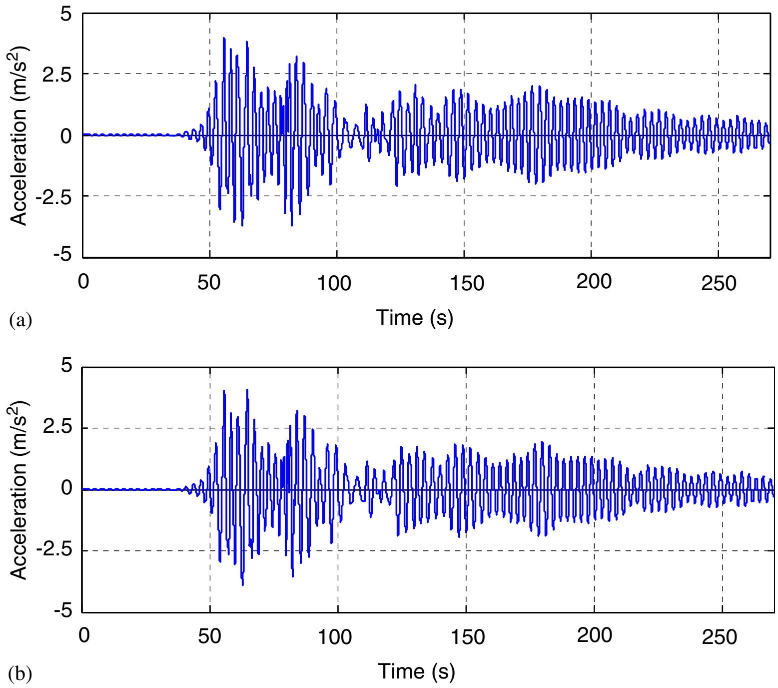

Figure 10. Responses of model in y direction: (a) response with model matching method and (b) response with H_∞ method.

By the convolution integration operation of the transfer function $T_{ru}(s)$ and the target wave r, the shaking table's input wave u can be obtained. Furthermore, the wave u is filtered by a lowpass digital Chebyshev filter to cut highfrequency components. Under the excitation of the generated waves, the responses of the simulation model were calculated by the time history analysis. The responses in the y direction are shown in Figure 10. Note that the compass directions associated with the axes are EW for the x direction and NS for the y direction. Comparing Figure 10 with Figure 4(c), it is notable that the model responses when using both the model matching method and the H_∞ method are in good agreement with the target wave. Based on the Fourier amplitude spectra, the error of reproduction is defined as follows:

$$Er = \frac{\sum(S_{\text{tar}} - S_{\text{res}})^2}{\sum(S_{\text{tar}})^2} \times 100\% \tag{13}$$

in which, S_{tar} and S_{res} represent the Fourier amplitude spectrum of the target wave and that of the model response, respectively. When using the model matching method, the reproduction errors were 2.9 and 4.8% in the x and y direction, respectively; while when using the H_∞ method, the reproduction errors were 4.6 and 6.9%. The results of the numerical example verify that the IDCS algorithm is effective, and both the model matching method and the H_∞ method are similar in the accuracy of the controller design. In the following shaking table tests, only the model matching method was used to construct the controller.

DOI: 10.1002/eqe

5. EXPERIMENTAL VALIDATION

5.1. Test specimen

To validate the techniques developed for the substructure shaking table test and to investigate the seismic behavior of furniture, a series of full-scale tests were conducted in E-Defense. As shown in Figure 11, a five-story steel frame was placed on a rubber-and-mass system. The steel frame had a plan dimension of 9 m by 12 m and a total height of 18.5 m. The story stiffness of the frame was very large (more than 100 times the stiffness of each rubber layer) so that the frame would behave

(a)

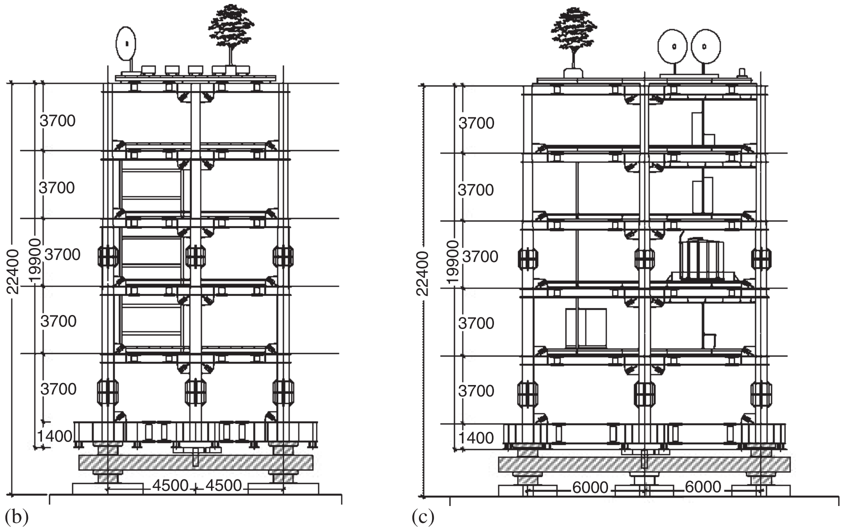

(b) (c)

Figure 11. Overview and drawings of test specimen: (a) specimen view; (b) elevation in x direction; and (c) elevation in y direction.

DOI: 10.1002/eqe

as a rigid body during the vibration. Five stories were used only to expand the floor areas available for furniture installation and make it possible to conduct many furniture tests simultaneously. After the installation of furniture, the total mass of the frame model weighted 3.95×10^5 kg.

Because the maximum displacement demand was larger than the drift (horizontal displacement) limit accepted by normal rubber bearings, two layers were adopted for the mass-and-rubber system. To achieve an approximately equal drift between the two layers, the stiffness ratio and the mass ratio between the first and second rubber layers were designed to be 1.5:1 and 1:1. Four rubber bearings were placed at the corners of each layer. All rubber bearings were 1000 mm in diameter and 285 mm in height. In reference to the weight of the test structure placed on top of the mass-and-rubber system, a mass of 3.60×10^5 kg was chosen for the lumped mass, which was made of a 0.8 m thick concrete slab of 12 by 15 m in plan. The horizontal stiffness was given as 1.37 and 0.878 MN/m for each rubber bearing in the first and second layers, which was achieved by the adjustment of the shear modulus of the rubber material.

5.2. Modal parameter identification

To understand the dynamic properties of the test specimen and validate the numerical model, system identification on the specimen was conducted before the seismic tests. A Gaussian white noise with a pass-band of 0.12$\sim$10 Hz, a root mean square (RMS) amplitude of 73 gal, and a duration of 250 s, was used as the input wave of the shaking table. The accelerations of both the excitation and response were recorded by servo accelerometers at an interval of 0.005 s. The transfer function was obtained as a quotient of the auto-spectral density of the output signal over the cross-spectral density of the input and output signals. In the signal processing, a digital filter was used to eliminate the measurement noise, a Hanning window was added to reduce the effects of leakage, and an averaging technique was adopted to reduce the relative standard deviation of the power spectra [29]. The transfer function from the base to the second floor of steel frame is shown in Figure 12. A frequency domain curve-fitting algorithm was employed to extract the modal parameters from the transfer function [29]. The identified modal frequencies were 0.35 and 0.98 Hz, close to the frequencies of the numerical model. The identified first modal damping ratio was 2.9%, which was fortuitously close to the assumed value in the numerical model.

5.3. Input wave of the shaking table

The input waves of the shaking table were generated from the numerical loop of the IDCS algorithm, based on the target waves and the numerical model of the test specimen. To save oil, the waves generated by the IDCS algorithm were filtered by a low-pass digital Chebyshev filter, in which the cutoff frequency was set at the second modal frequency. To ensure the safety and feasibility of the actual tests, the input waves had to be inspected carefully to satisfy the following restrictions: (1) the displacement, velocity, and acceleration capacity of the shaking table; (2) the oil supply limit of the shaking table; (3) the drift limit of the rubber bearings; (4) the tension limit of the rubber bearings. The displacement and velocity of the shaking table can be calculated by integrating the acceleration wave, and the demand for oil is related to the cumulative displacement of table. The procedure to calculate the oil demand can be found in Reference [14]. The drifts of the rubber bearings can be estimated from the time history analysis of the numerical model, and the tension forces extended to the rubber bearings can be obtained from the estimated overturning moment.

DOI: 10.1002/eqe

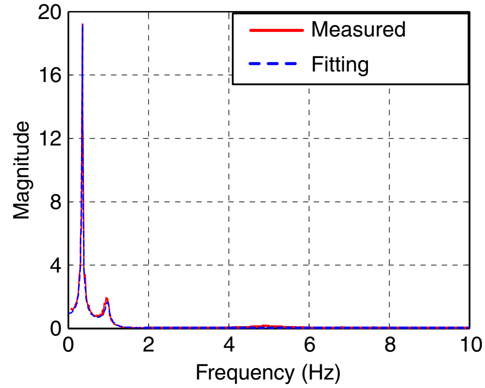

Figure 12. Transfer function curve of test specimen.

Table II. Inspection of shaking table's input waves.

	Displacement (m)	Velocity (m/s)	Oil supply (kl)	Drift (m)		Rubber tension (kN)	
				Layer 1	Layer 2	Layer 1	Layer 2
Limit	1.0	2.0	20.0	0.75	0.75	784	784
100% case	0.40	0.75	26.2	0.46	0.49	−659	9
80% case	0.32	0.60	17.9	0.37	0.40	−897	−187

For 100 and 80% of the response at the top floor of the 30-story building, the demands and capacities are summarized in Table II. The table indicates that for the 100% case, the requirement for oil is not satisfactory, while for the 80% case, all restrictions are removed. Thus, 80% of the top floor's response was chosen as the target response of the test specimen. The associated input wave for the shaking table test is shown in Figure 13.

5.4. Test results

During shaking, the accelerations of the test specimen's floors were recorded by servo accelerometers at an interval of 0.005 s. The recorded data revealed that the floor accelerations were nearly identical for all the five floors, with the differences not greater than 1%. Figure 14 shows the acceleration response at the second floor and the target wave in the y direction. The corresponding Fourier amplitude spectra obtained from the fast Fourier transform are shown in Figure 15. From these figures, good correlation between the specimen's response and the target wave is notable. A similar observation was also obtained from the acceleration data in the x direction. The reproduction errors estimated by Equation (13) were 11.1 and 16.2% in the x and y direction, respectively. Comparison of the floor response with the table input indicates that the rubber-and-mass system is capable of amplifying the table motion significantly. The maximum velocity and displacement were amplified to 3.4 and 3.6 times, respectively.

DOI: 10.1002/eqe

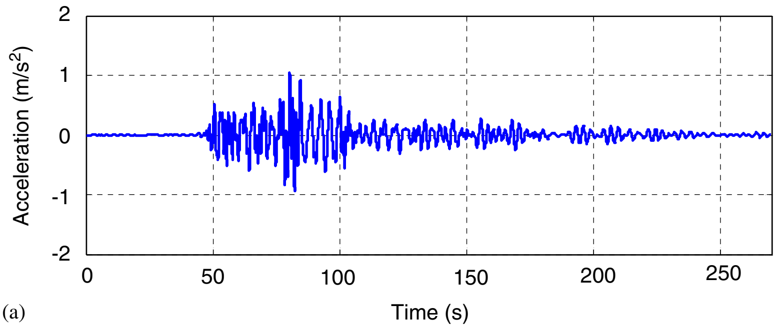

(a)

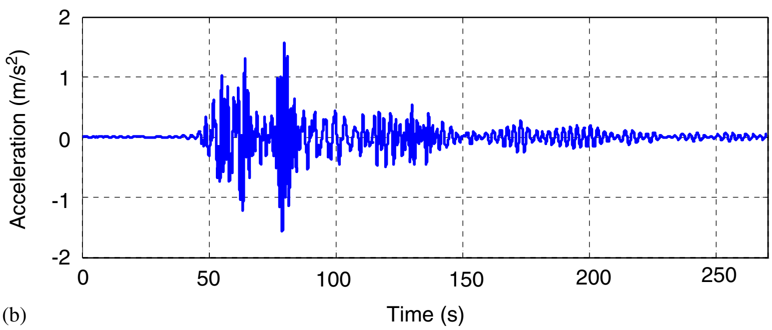

(b)

Figure 13. Time history of shaking table's input wave: (a) x direction and (b) y direction.

The reproduction errors in the test were larger than those in the numerical example. It occurred because of the shaking table's control and the modeling error for the test specimen, in addition to the measurement noise. The errors of the Fourier amplitude spectra between the designed input waves and the measured accelerations of the shaking table were very small, being 2.0 and 1.6% in the x and y direction. The modeling error for the test specimen, e.g. the neglect of the nonlinearity of rubbers, was speculated to be the main source of reproduction errors.

5.5. Seismic behaviors of furniture

Various types of furnitures were installed on the test specimen's floors, which simulated rooms with different functions, e.g. an office set on the second floor, a bed room set on the third floor, and a living room and kitchen set on the fourth floor. In the simulated offices, furniture set on the left span was placed naturally on the floor, while the furniture set on the right span was clamped on the floor or to the partition wall by small channel steels and bolts.

The damage to the furniture is briefly summarized as follows. Most of the furniture not clamped to the floor or wall overturned under large floor responses. Some scenes after shaking are shown in Figure 16. Compared with that furniture, the set of furniture clamped on the floor or wall exhibited noticeably better performance, not causing overturning as shown in Figure 16(a). This demonstrated the effectiveness of clamping. Note that in this test a floor response even larger than that described in the previous subsection was adopted. The detail of the furniture damage together with the adopted motion will be the subject of the companion paper.

DOI: 10.1002/eqe

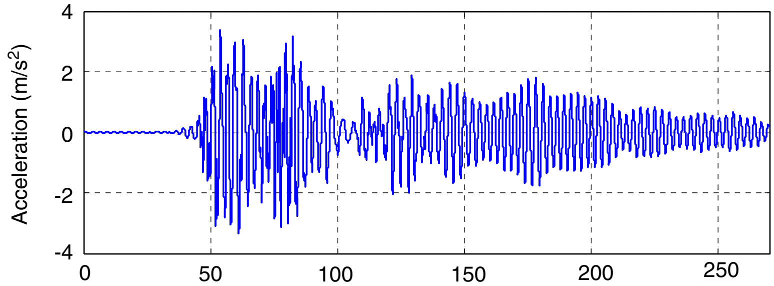

(a)

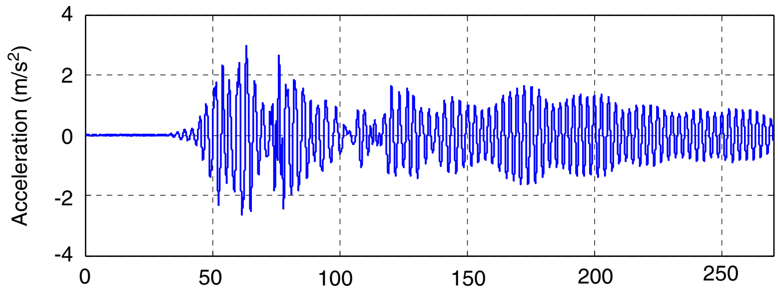

(b)

Figure 14. Time history of target wave and specimen's response in y direction: (a) target wave and (b) response of specimen.

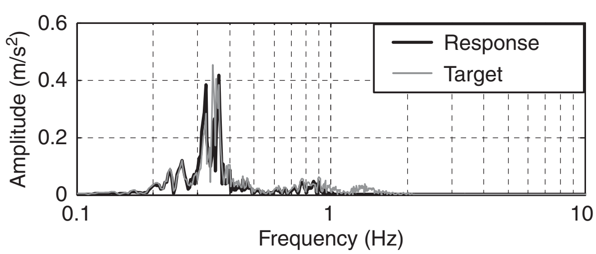

Figure 15. Fourier amplitude spectra of target wave and specimen's response in y direction.

6. CONCLUSIONS

In this study, a full-scale substructure shaking table test is developed to reproduce the response of the top floor of a high-rise building when it is subjected to long-period, long-duration ground motion. Here, the top floor is extracted as the test specimen. To overcome the capacity limitations of a shaking table, a rubber-and-mass system is proposed to amplify the motion of the shaking table. An open-loop IDCS algorithm is employed to generate the input wave of the shaking table to achieve an accurate reproduction of the floor response. A numerical example and shaking table tests were performed to illustrate and validate the developed techniques.

DOI: 10.1002/eqe

Figure 16. Damage to furniture after shaking: (a) office where furniture is clamped; (b) office where furniture is not fixed; (c) living room; and (d) kitchen.

The following conclusions are drawn from this study. (1) The designed rubber-and-mass system is capable of amplifying the input waves of the shaking table effectively. (2) The open-loop IDCS algorithm can generate suitable input waves of the shaking table by building an accurate numerical model and constructing a good controller. Both the model matching method and the H_∞ method show good performance for the controller design. (3) Using the input waves generated by the IDCS algorithm, the responses at the top floor of a high-rise building were reproduced reasonably by the substructure shaking table test.

Comparisons of the results between the physical test and the numerical simulation show that the reproduction errors mainly result from the modeling errors of the rubber bearings, especially the neglect of their nonlinearity. It should be pointed out that the control algorithm used in this study is offline and does not consider the nonlinearity of the test specimen. Room for improvement does exist in the development of the substructure shaking table test, including (1) development of a control algorithm that can handle the nonlinearity of the test specimen; and (2) development of a real-time feedback control that would allow elimination of the adverse influence of modeling errors.

ACKNOWLEDGEMENTS

The Committee on Disaster Mitigation Research using E-Defense (chaired by Prof. Tsuneo Okada) provided valuable suggestions for the work described in this paper. The authors would like to extend their

DOI: 10.1002/eqe

sincere gratitude to the committee. The authors would also like to thank the anonymous reviewers for their valuable comments and suggestions.

REFERENCES

1. Kamae K, Kawabe H, Irikura K. Strong ground motion prediction for huge subduction earthquakes using a characterized source model and several simulation techniques. *Proceedings of the 13th World Conference on Earthquake Engineering*, Vancouver, 2004; Paper No.655.
2. Suita K, Kitamura Y, Gotoh T, Iwata T, Kamae K. Seismic response of high-rise buildings constructed in 1970s subjected to long-period ground motions. *Journal of Structural and Construction Engineering* (Transaction of AIJ) 2007; **611**:55–61 (in Japanese).
3. Masatsuki T, Midorikawa S, Ohori M, Miura H. Simulation for seismic behavior of office furniture in a high-rise building. *Journal of Structural and Construction Engineering* (Transaction of AIJ) 2007; **620**:43–49 (in Japanese).
4. Ghaboussi J, Yun G, Hashash Y. A novel predictor–corrector algorithm for sub-structure pseudo-dynamic testing. *Journal of Earthquake Engineering and Structural Dynamics* 2006; **35**:453–476.
5. Elkhoraibi T, Mosalam KM. Towards error-free hybrid simulation using mixed variables. *Journal of Earthquake Engineering and Structural Dynamics* 2007; **36**:1497–1522.
6. Wang KJ, Tsai KC, Wang SJ, Cheng WC, Yang YS. ISEE: Internet-based simulation for earthquake engineering. Part II: the application protocol approach. *Journal of Earthquake Engineering and Structural Dynamics* 2007; **36**:2307–2323.
7. Wang T, Yoshitake N, Pan P, Lee TH, Nakashima M. Numerical characteristics of peer-to-peer (P2P) internet online hybrid test system and its application to seismic simulation of SRC structure. *Journal of Earthquake Engineering and Structural Dynamics* 2008; **37**:265–282.
8. Wang T, McCormick J, Yoshitake N, Pan P, Murata Y, Nakashima M. Collapse simulation of a four-story steel moment frame by a distributed online hybrid test. *Journal of Earthquake Engineering and Structural Dynamics* 2008; **37**:955–974.
9. Nakashima M, Kato H, Takaoka E. Development of real-time pseudo dynamic testing. *Journal of Earthquake Engineering and Structural Dynamics* 1992; **21**:79–92.
10. Bonnet PA, Lim CN, Williams MS, Blakeborough A, Neild SA, Stoten DP, Taylor CA. Real-time hybrid experiments with Newmark integration, MCSmd outer-loop control and multi-tasking strategies. *Journal of Earthquake Engineering and Structural Dynamics* 2007; **36**:119–141.
11. Chen C, Ricles JM. Stability analysis of SDOF real-time hybrid testing systems with explicit integration algorithms and actuator delay. *Journal of Earthquake Engineering and Structural Dynamics* 2008; **37**:597–613.
12. Ahmadizadeh M, Mosqueda G, Reinhorn AM. Compensation of actuator delay and dynamics for real-time hybrid structural simulation. *Journal of Earthquake Engineering and Structural Dynamics* 2008; **37**:21–42.
13. Mercan O, Ricles JM. Stability analysis for real-time pseudodynamic and hybrid psedodynamic testing with multiple sources of delay. *Journal of Earthquake Engineering and Structural Dynamics* 2008; **37**:1269–1293.
14. Nagae T, Kajiwara K, Fujitani H, Fukuyama K, Kawabe H, Ohnishi K, Kido S, Nakashima M. Test on seismic response of high-rise building focusing on furniture and non-structural components. *Journal of Structural and Construction Engineering* (Transaction of AIJ) 2008; **628**:1007–1014 (in Japanese).
15. Nakashima M. Test on collapse behavior of structural systems. *Science and Technology in Japan* 2006; **96**:14–19.
16. Tagawa Y, Kajiwara K. Controller development for the E-Defense shaking table. *Proceedings of the Institution of Mechanical Engineers*, *Part I*: *Journal of System and Control Engineering* 2007; **221**(2):171–181.
17. Nield SA, Stoten DP, Drury D, Wagg DJ. Control issues relating to real-time substructuring experiments using a shaking table. *Journal of Earthquake Engineering and Structural Dynamics* 2005; **34**:1171–1192.
18. Tagawa Y, Fukui K. Inverse dynamics calculation of nonlinear model using low sensitivity compensator. *Proceedings of Dynamics and Design and Conference*, Akita, 1994; 185–188 (in Japanese).
19. Tu J. *Control of Nonlinear System Using the Inverse Dynamics Compensation via Simulation* (*IDCS*) *Method*. University of Bristol: Bristol, 2007.
20. Ichikawa K. *Control System Design Based on Exact Model Matching Techniques*. Springer: Berlin, 1985.
21. Zhou K, Doyle JC, Glover K. *Robust and Optimal Control*. Prentice-Hall: New Jersey, 1996.
22. Bott R, Duffin RJ. On the algebra of networks. *Transactions of the American Mathematical Society* 1953; **74**:99–109.
23. Spence Jr BF, Suhardjo J, Sain MK. Frequency domain optimal control strategies for aseismic protection. *Journal of Engineering Mechanics* (ASCE) 1994; **120**(1):135–158.

DOI: 10.1002/eqe

24. Tsai MC, Geddes EJM, Postlethwaite I. Pole-zero cancellations and closed-loop properties of an H_∞ mixed sensitivity design problem. *Automatica* 1992; **28**(3):519–530.
25. Doyle JC, Francis BA, Tannenbaum AR. *Feedback Control Theory*. Macmillan Publishing Company: New York, 1992.
26. Safonov MG, Limerbeer DJN, Chiang RY. Simplifying the H_∞ theory via loop-shifting, matrix-pencil and descriptor concepts. *International Journal of Control* 1989; **50**(6):2467–2488.
27. Chiang RY, Safonov MG. *Robust Control Toolbox User's Guide*. The MathWorks, 1996.
28. Ogata K. *Modern Control Engineering*. Prentice-Hall Inc.: New Jersey, 2002.
29. Ewins DJ. *Modal Testing*: *Theory*, *Practice and Application* (2nd edn). Taylor & Francis: London, 2000.

DOI: 10.1002/eqe